Ceramic Binder Jetting Additive Manufacturing: Relationships among Powder Properties, Feed Region Density, and Powder Bed Density

Ming Li

xaviorsbear2015@tamu.edu

Department of Industrial and Systems Engineering, Texas A&M University, College Station, TX, US

Guanxiong Miao

gm2666@tamu.edu

Department of Mechanical Engineering, Texas A&M University, College Station, TX, US

Mohammadamin Moghadasi

moghadasi.m@tamu.edu

Department of Materials Science and Engineering, Texas A&M University, College Station, TX, US

Zhijian Pei

zjpei@tamu.edu

Department of Industrial and Systems Engineering, Texas A&M University, College Station, TX, US

Chao Ma*

cma@tamu.edu

Department of Industrial and Systems Engineering, Texas A&M University, College Station, TX, US

Department of Mechanical Engineering, Texas A&M University, College Station, TX, US

Department of Materials Science and Engineering, Texas A&M University, College Station, TX, US

Department of Engineering Technology and Industrial Distribution, Texas A&M University, College Station, TX, US

* Corresponding author. E-mail address: cma@tamu.edu. Postal address: 3367 TAMU, College Station, TX 77843-3367, US.

Abstract

This short communication reports an experimental investigation on the relationships among powder properties (i.e., apparent density, tap density, and Hausner ratio), feed region density, and powder bed density in ceramic binder jetting additive manufacturing. Seven differently sized alumina powders (from 0.05 μm to 70 μm) were used for this experimental investigation. Simple linear regression was applied to analyze the experimental data. It was found that powder bed density matched well with feed region density under all conditions of this investigation. The results also showed that apparent density was a stronger predictor than tap density and Hausner ratio for powder bed density.

Keywords: *Additive manufacturing; binder jetting; alumina; powder properties; feed region density; powder bed density*

1. Introduction

Ceramic binder jetting additive manufacturing has attracted increasing attention from a large range of industries, such as healthcare, aerospace, and energy [1]. Powder bed density plays an important role in ceramic binder jetting additive manufacturing. Green density, which determines the density of final parts, is directly affected by powder bed density [1, 2]. The selection of binder saturation also depends on powder bed density. Therefore, understanding and predicting powder bed density is essential to controlling the performance of ceramic parts produced by binder jetting additive manufacturing.

To date, it is still difficult to predict powder bed density for a new powder a priori (i.e., before powder spreading). Directly measuring powder bed density for a new powder is not efficient

because it leads to increased machine usage time and higher labor cost. Some models have been developed to predict powder bed density using the discrete element method [3-8]. But numerical models also rely on experimental measurements to be calibrated for a specific powder. Several researchers adopted powder properties such as apparent density, tap density, or Hausner ratio to infer powder bed density [9-17]. There has been, nevertheless, no conclusive results demonstrating whether one of these powder properties could offer an accurate prediction of powder bed density.

This study aims to reveal the relationships among powder properties (apparent density, tap density, or Hausner ratio), feed region density, and powder bed density, and to identify an effective predictor for powder bed density a priori. In this paper, apparent density specifically refers to the density of freely settled powder. Apparent density is measured with a Hall funnel and a standard density cup. Tap density refers to the density of a powder that has been tapped, to settle contents, in a container under specified conditions. Hausner ratio is the ratio of tap density to apparent density. Feed region density refers to the density of powder that has filled the feed region of the 3D printer. Powder bed density refers to the density of the powder bed that is formed by the powder spreading process on the build platform of the 3D printer. Feed region density and powder bed density are measured through the weight and volume of the powder in the feed region and on the build platform, respectively.

2. Materials and Methods

A comprehensive study on powder bed density was carried out on alumina powders with a wide range of nominal particle sizes from 0.05 μm to 70 μm. The specific information of each alumina powder is listed in Table 1.

Table 1. Alumina powders used in this study

Nominal particle size (μm)	Supplier	Item number
0.05	Allied High Tech Products	90-187050
0.3	Allied High Tech Products	90-187125
2	Inframat	26R-8S02
10	Inframat	26R-8S10
20	Inframat	26R-8S20
40	Inframat	26R-8S40
70	Inframat	26R-8S70

The particle size distribution of each alumina powder was measured using a HORIBA LA-960 laser scattering machine. To represent the state of powder used in binder jetting additive manufacturing, measurement of particle size was conducted on dry powders directly. Each measurement was repeated three times. The powder morphology of each alumina powder was characterized with scanning electron microscopes (SEM), including JEOL JSM-7500F and TESCAN FERA3.

The powder properties investigated in this study are apparent density, tap density, and Hausner ratio. The measurement of apparent density was conducted using a Hall funnel and a density cup, following the ASTM B212-17 standard [18]. The tap density of each powder was measured by tapping the powder 3000 times according to the ASTM B527-15 standard [19]. The mass of powder was measured by a balance with a resolution of 0.001 g. Hausner ratio, i.e., the ratio of tap density to apparent density, was then calculated.

A commercial binder jetting 3D printer (ComeTrue T10, Microjet Technology) was used for powder spreading. Custom devices were designed and installed on the printer for measuring feed region density and powder bed density. As shown in Figure 1, two sets of custom devices (orange components) are installed onto the feed region platform and build platform of the original printer (grey components), respectively. Each set of the devices consisted of an insert that was aligned

with the top of the feed region or the build region, and a piston that was fixed to the original piston to carry out the same downward or upward movement during powder spreading. The dimensions of the two custom pistons were the same (25×25 mm^2).

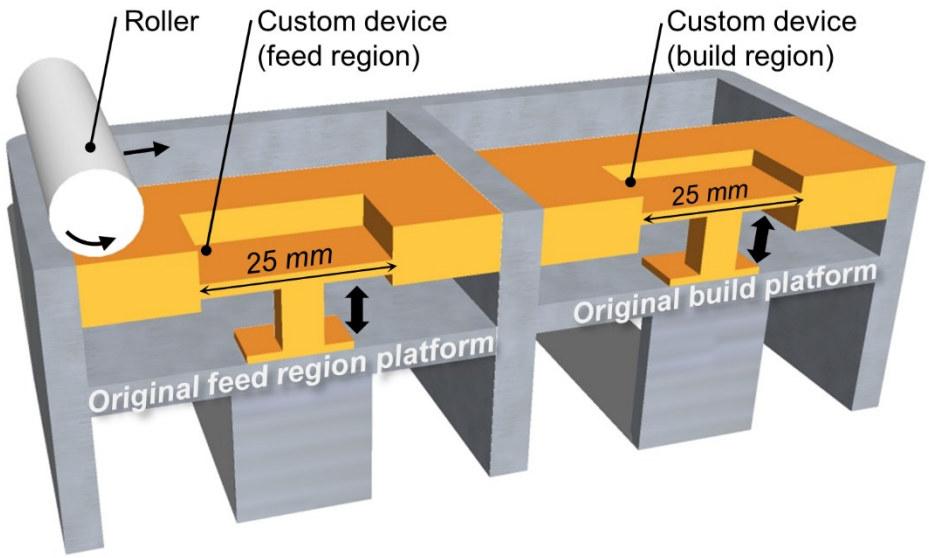

Figure 1. Schematic illustration of the cross-section of the 3D printer and custom devices for measurements of feed region density and powder bed density

In each powder spreading experiment, a Hall funnel was utilized to fill the feed region with the powder. The outlet of the Hall funnel was maintained at 88 mm above the center of the feed region. The powder then flowed from the Hall funnel until it completely filled the feed region. After removing the excess powder by a glass slide, the heights of four corners in the feed region were measured by a caliper with a resolution of 0.01 mm. The relative feed region density (ρ'_{fr}) was calculated using Equation (1):

$$\rho'_{fr} = \frac{m_{fr}}{h_{fr} A_{fr} \rho_{th}} \quad (1)$$

where m_{fr} is the mass of powder in the feed region, h_{fr} is the average powder height of the feed region, A_{fr} is the area of the feed region, and ρ_{th} is the theoretical density of alumina (3.97 g/cm^3) [20].

Powder spreading was carried out to form a powder bed with a desired height of 10.08 mm (63 layers) by a counter-rotating roller. The spreading parameters were chosen to ensure a full powder coverage for all powders and kept constant for all measurements, as listed in Table 2. After powder spreading was finished, a glass slide was used to remove the powder in the clearance between the roller and the custom device on the build platform. Similar to the measurement of feed region density, the heights of four corners in the powder bed were measured. The relative powder bed density (ρ'_{pb}) was then calculated by Equation (2):

$$\rho'_{pb} = \frac{m_{pb}}{h_{pb} A_{pb} \rho_{th}} \quad (2)$$

where m_{pb} is the mass of powder in the build region, h_{pb} is the average height of powder in the build region, and A_{pb} is the area of the build region. Each powder density measurement was repeated three times.

Table 2. Parameters used in powder spreading experiments for all seven alumina powders

Parameter	Value
Layer thickness (mm)	0.16
Dosing ratio	1.4
Roller traverse speed (mm/s)	50
Roller rotational speed (rpm)	500

3. Results and Discussion

The particle size distributions for all seven alumina powders measured by the laser scattering machine are presented in Figure 2. Because of the usage of dry powders for particle size

distribution measurement, the powders with nominal particle sizes of 0.05 μm and 0.3 μm exhibit much larger measured particle sizes than the nominal values and wide particle size ranges. This is indicative of the presence of agglomeration for these two fine powders. For the other five coarser powders, the median particle sizes (D_{50}) are close to their nominal values.

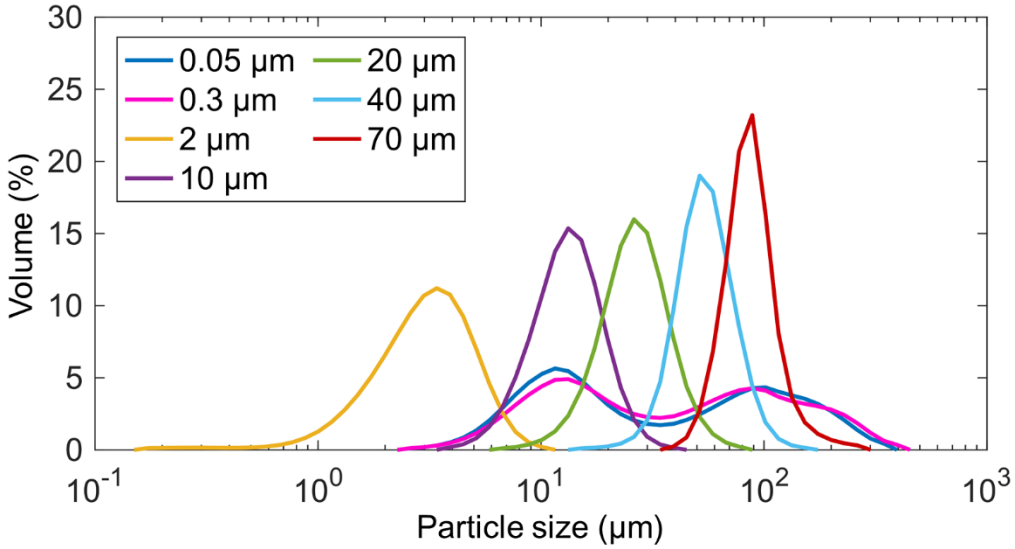

Figure 2. Particle size distribution of all seven alumina powders used in this study

The morphology of each powder is shown in Figure 3. As can be seen from the micrographs, powders with larger particle sizes exhibit a high degree of sphericity. The powders with the nominal particle sizes of 0.05 μm and 0.3 μm form agglomerates with varying sizes, which is consistent with the observations from particle size distribution measurements shown in Figure 2.

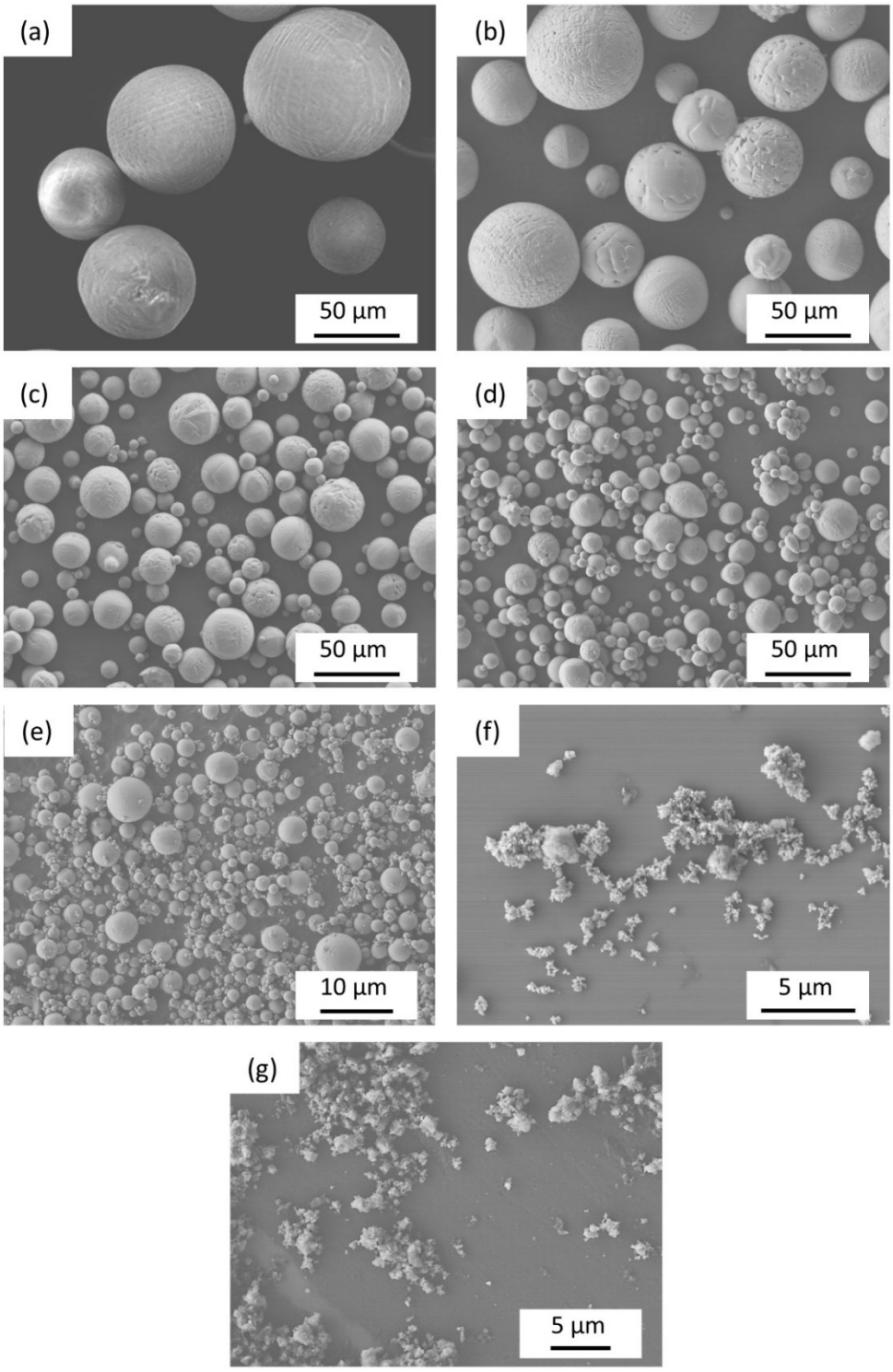

Figure 3. Scanning electron micrographs of all seven alumina powders of different nominal particle sizes of (a) 70 µm, (b) 40 µm, (c) 20 µm, (d) 10 µm, (e) 2 µm, (f) 0.3 µm, and (g) 0.05 µm

Figure 4 shows density measurement results for all seven alumina powders with different nominal particle sizes (0.05 μm, 0.3 μm, 2 μm, 10 μm, 20 μm, 40 μm, and 70 μm). The apparent density, feed region density, and powder bed density share a similar upward trend with increasing particle size. As particle size increases from 0.05 μm to 70 μm, apparent density, feed region density, and powder bed density increase significantly, from 1.6% to 52.6%, from 1.9% to 53.8%, and from 1.8% to 53.1%, respectively. Tap density, on the other hand, is consistently much higher than the other measured powder densities for all particle sizes. Tap density has a significant growth from 4.2% to 58.1% when particle size increases from 0.05 μm to 2 μm. Then tap density reaches a plateau upon a further increase in particle size from 2 μm to 70 μm.

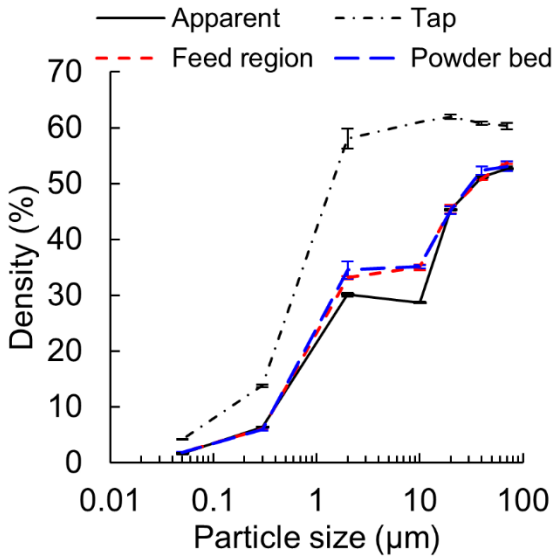

Figure 4. Apparent density, tap density, feed region density, and powder bed density at nominal particle sizes from 0.05 μm to 70 μm

Figure 5a shows powder bed density as a function of feed region density. A linear regression model with an intercept of 0 was used to fit the data, resulting in a slope of about 1 and a very high adjusted R^2 value of 0.9996, shown as the dotted line. This pronounced positive proportional

relationship between feed region density and powder bed density suggests that powder bed density matches very well with feed region density.

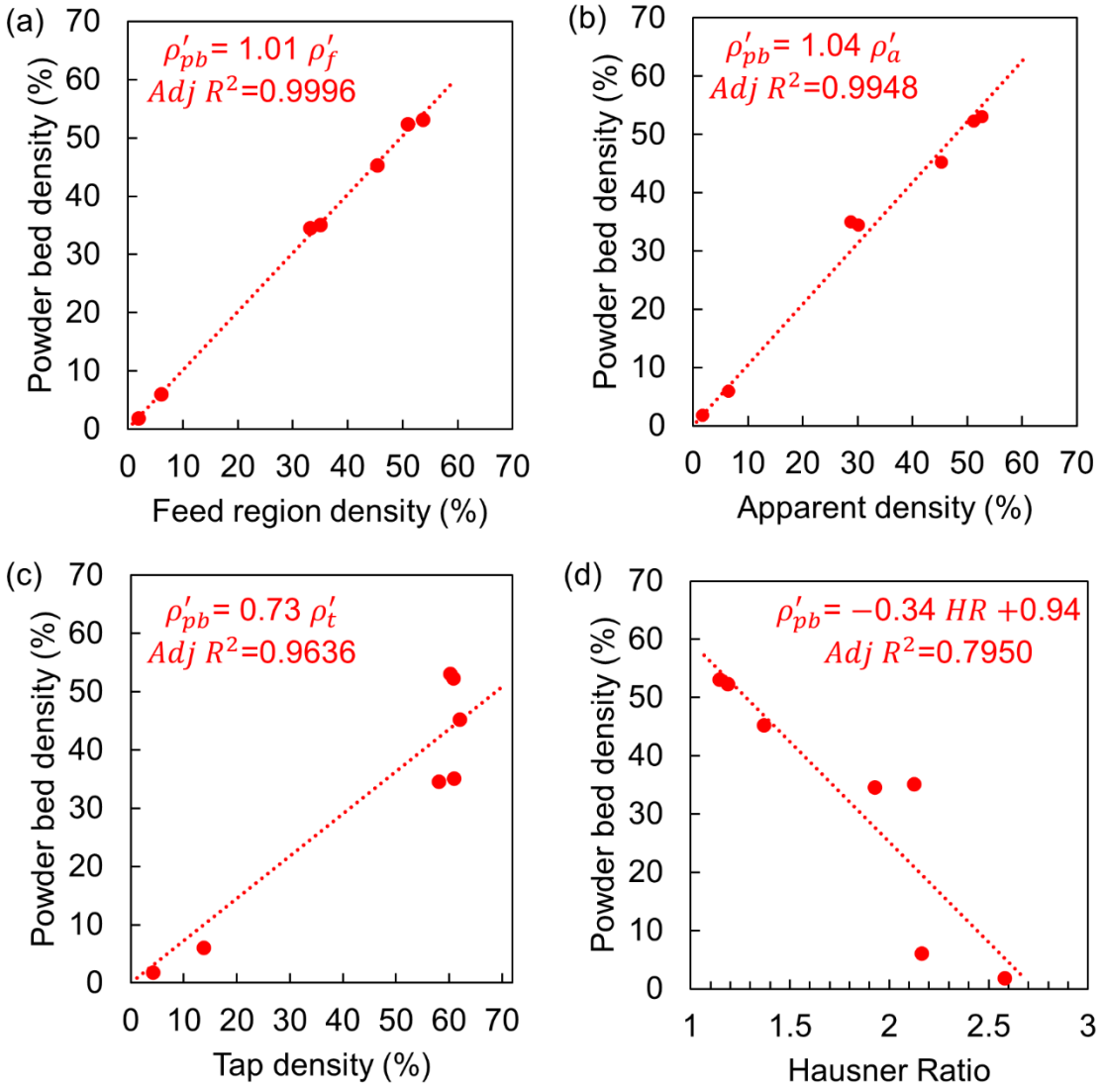

Figure 5. Powder bed density as a function of (a) feed region density, (b) apparent density, (c) tap density, and (d) Hausner ratio, respectively

Figure 5b shows the relationship between apparent density and powder bed density. The data obtained in this study were fitted by a linear regression model with an intercept of 0 (red dotted line), resulting in a high adjusted R^2 value of 0.9948 and a slope approximately equal to 1.

Figure 5c shows the relationship between tap density and powder bed density. A linear regression model with an intercept of 0 (red dotted line) was fitted by the data obtained in this study. With some points deviating from the line, the adjusted R^2 value for this model is 0.9636, lower than that for the apparent density model.

Figure 5d is plotted to show the relationship between Hausner ratio and powder bed density. Regressed by the data from this study, the fitted linear model possesses a negative slope of –0.34 and an intercept of 0.94. It is clear that the adjusted R^2 value of 0.7950 for this model is the lowest among all simple linear regression models in this study.

In order to further compare the prediction errors of these three simple linear regression models of powder bed density based on different powder properties, the Akaike information criterion (AIC) was used to evaluate these models. The AIC criterion is known as an effective estimator for ranking model quality and inferring significant variables via the analysis of maximum likelihood [21, 22]. Due to the finite sample size, the corrected AIC criterion (AICc) was used on the models. The better the model is, the smaller the AICc score is. As can be seen in Table 3, the AICc score of the apparent density model is the lowest among the three models, followed by the tap density model and the Hausner ratio model. In addition, the mean squared error (MSE) was calculated. The result also suggests that, across the three linear regression models, the apparent density model demonstrates the best prediction performance. According to the AICc and MSE, apparent density can be identified as the most effective indicator among the measured powder properties.

Table 3. Comparisons of three simple linear regression models for powder bed density

Predictor	Prediction error	
	AICc	MSE
Apparent density (ρ_a')	44.89	15.58
Tap density (ρ_t')	58.50	44.92
Hausner ratio (HR)	75.01	64.31

4. Conclusions

This paper reports an experimental study on relationships between feed region density and powder bed density, and between powder properties (i.e., apparent density, tap density, and Hausner ratio) and powder bed density. Two major conclusions can be drawn:

1) powder bed density and feed region density match well with each other under all conditions of this study;

2) apparent density is a stronger predictor than tap density and Hausner ratio for powder bed density.

The new knowledge can be used to estimate powder bed density a priori from powder properties.

Declaration of Competing Interest

The authors declare that they have no known competing financial interests or personal relationships that could have appeared to influence the work reported in this paper.

Acknowledgement

This material is based upon work supported by the National Science Foundation (Grant No. 1762341).

References

[1] Du, W., Ren, X., Pei, Z., and Ma, C., 2020, "Ceramic binder jetting additive manufacturing: a literature review on density," Journal of Manufacturing Science Engineering, 142(4).

[2] Li, M., Du, W., Elwany, A., Pei, Z., and Ma, C., 2020, "Metal binder jetting additive manufacturing: A literature review," Journal of Manufacturing Science Engineering, pp. 1-45.

[3] Haeri, S., 2017, "Optimisation of blade type spreaders for powder bed preparation in additive manufacturing using DEM simulations," Powder Technology, 321, pp. 94-104.

[4] Haeri, S., Wang, Y., Ghita, O., and Sun, J., 2017, "Discrete element simulation and experimental study of powder spreading process in additive manufacturing," Powder Technology, 306, pp. 45-54.

[5] Chen, H., Wei, Q., Wen, S., Li, Z., and Shi, Y., 2017, "Flow behavior of powder particles in layering process of selective laser melting: Numerical modeling and experimental verification based on discrete element method," International Journal of Machine Tools Manufacture, 123, pp. 146-159.

[6] Nan, W., Pasha, M., and Ghadiri, M., 2020, "Numerical simulation of particle flow and segregation during roller spreading process in additive manufacturing," Powder Technology, 364, pp. 811-821.

[7] Meier, C., Weissbach, R., Weinberg, J., Wall, W. A., and Hart, A. J., 2019, "Critical influences of particle size and adhesion on the powder layer uniformity in metal additive manufacturing," Journal of Materials Processing Technology, 266, pp. 484-501.

[8] Parteli, E. J., and Pöschel, T., 2016, "Particle-based simulation of powder application in additive manufacturing," Powder Technology, 288, pp. 96-102.

[9] Bai, Y., Wagner, G., and Williams, C. B., 2015, "Effect of bimodal powder mixture on powder packing density and sintered density in binder jetting of metals," 2015 Annual International Solid Freeform Fabrication Symposium, pp. 758-771.

[10] Bai, Y., Wagner, G., and Williams, C. B., 2017, "Effect of particle size distribution on powder packing and sintering in binder jetting additive manufacturing of metals," Journal of Manufacturing Science and Engineering, 139(8), pp. 1–6.

[11] Turker, M., Godlinski, D., and Petzoldt, F., 2008, "Effect of production parameters on the properties of IN 718 superalloy by three-dimensional printing," Materials Characterization, 59(12), pp. 1728-1735.

[12] Inaekyan, K., Paserin, V., Bailon-Poujol, I., and Brailovski, V., 2016, "Binder-jetting additive manufacturing with water atomized iron powders," AMPM 2016 Conference on Additive Manufacturing, pp. 5-7.

[13] Yoo, H. J., 1997, "Reactive binders for metal parts produced by three dimensional printing," Massachusetts Institute of Technology.

[14] Lv, X., Ye, F., Cheng, L., Fan, S., and Liu, Y., 2019, "Fabrication of SiC whisker-reinforced SiC ceramic matrix composites based on 3D printing and chemical vapor infiltration technology," Journal of the European Ceramic Society, 39(11), pp. 3380-3386.

[15] Meenashisundaram, G. K., Wang, N., Maskomani, S., Lu, S., Anantharajan, S. K., Dheen, S. T., Nai, S. M. L., Fuh, J. Y. H., and Wei, J., 2020, "Fabrication of Ti+ Mg composites by three-dimensional printing of porous Ti and subsequent pressureless infiltration of biodegradable Mg," Materials Science and Engineering: C, 108, p. 110478.

[16] Miao, G., Du, W., Moghadasi, M., Pei, Z., and Ma, C., 2020, "Ceramic binder jetting additive manufacturing: Effects of granulation on properties of feedstock powder and printed and sintered parts," Additive Manufacturing, p. 101542.

[17] Moghadasi, M., Du, W., Li, M., Pei, Z., and Ma, C., 2020, "Ceramic binder jetting additive manufacturing: Effects of particle size on feedstock powder and final part properties," Ceramics International, pp. 16966-16972.

[18] ASTM Standard, 2017, B212-17: Standard Test Method for Apparent Density of Free Flowing Metal Powders using the Hall Flowmeter Funnel.

[19] ASTM Standard, 2015, B527-15: Standard Test Method for Tap Density of Metal Powders and Compounds.

[20] Geldart, D., Harnby, N., and Wong, A., 1984, "Fluidization of cohesive powders," Powder Technology, 37(1), pp. 25-37.

[21] Burnham, K. P., and Anderson, D. R., 2004, "Multimodel inference: understanding AIC and BIC in model selection," Sociological methods & research, 33(2), pp. 261-304.

[22] Akaike, H., 1987, "Factor analysis and AIC," Selected papers of hirotugu akaike, Springer, pp. 371-386.

Figure Captions

Figure 1. Schematic illustration of the cross-section of the 3D printer and custom devices for measurements of feed region density and powder bed density

Figure 2. Particle size distribution of all seven alumina powders used in this study

Figure 3. Scanning electron micrographs of all seven alumina powders of different nominal particle sizes (a) 70 μm, (b) 40 μm, (c) 20 μm, (d) 10 μm, (e) 2 μm, (f) 0.3 μm, and (g) 0.05 μm

Figure 4. Apparent density, tap density, feed region density, and powder bed density at nominal particle sizes from 0.05 μm to 70 μm

Figure 5. Powder bed density as a function of (a) feed region density, (b) apparent density, (c) tap density, and (d) Hausner ratio, respectively

Tables

Table 1. Alumina powders used in this study

Nominal particle size (μm)	Supplier	Item Number
0.05	Allied High Tech Products	90-187050
0.3	Allied High Tech Products	90-187125
2	Inframat	26R-8S02
10	Inframat	26R-8S10
20	Inframat	26R-8S20
40	Inframat	26R-8S40
70	Inframat	26R-8S70

Table 2. Parameters used in powder spreading experiments for all seven alumina powders

Parameter	Value
Layer thickness (mm)	0.16
Dosing ratio	1.4
Roller traverse speed (mm/s)	50
Roller rotational speed (rpm)	500

Table 3. Comparisons of three simple linear regression models for powder bed density

Predictor	Prediction error	
	AICc	MSE
Apparent density (ρ_a')	44.89	15.58
Tap density (ρ_t')	58.50	44.92
Hausner ratio (HR)	75.01	64.31